Pergamon

Prediction of tool and chip temperature in continuous and interrupted machining

Ismail Lazoglu *, Yusuf Altintas

Manufacturing Automation Laboratory, Department of Mechanical Engineering, University of British-Columbia, Vancouver, B.C. V6T1Z4, Canada

Abstract

In this paper, a numerical model based on the finite difference method is presented to predict tool and chip temperature fields in continuous machining and time varying milling processes. Continuous or steady state machining operations like orthogonal cutting are studied by modeling the heat transfer between the tool and chip at the tool—rake face contact zone. The shear energy created in the primary zone, the friction energy produced at the rake face—chip contact zone and the heat balance between the moving chip and stationary tool are considered. The temperature distribution is solved using the finite difference method. Later, the model is extended to milling where the cutting is interrupted and the chip thickness varies with time. The time varying chip is digitized into small elements with differential cutter rotation angles which are defined by the product of spindle speed and discrete time intervals. The temperature field in each differential element is modeled as a first-order dynamic system, whose time constant is identified based on the thermal properties of the tool and work material, and the initial temperature at the previous chip segment. The transient temperature variation is evaluated by recursively solving the first order heat transfer problem at successive chip elements. The proposed model combines the steady-state temperature prediction in continuous machining with transient temperature evaluation in interrupted cutting operations where the chip and the process change in a discontinuous manner. The mathematical models and simulation results are in satisfactory agreement with experimental temperature measurements reported in the literature.
© 2002 Published by Elsevier Science Ltd.

Keywords: Machining; Temperature; Finite difference

1. Introduction

The importance of temperature prediction for the machining processes has been well recognized in the machining research community primarily due to its effects on tool wear and its constraints on the productivity. It is well observed that particularly the rate of wear is greatly dependent on the tool–chip interface temperature [20]. Temperature is one of the major concerns and, after chatter stability, perhaps is the main limitation in the selection of process parameters, such as cutting speed and feedrate, in the machinability and production of some advanced materials such as titanium and nickel-based alloys [4]. In these materials, due to

their low thermal conductivity, most of the heat generated during the machining flows into the tool and, therefore, besides mechanical stresses on the cutting tools, severe thermal stresses occur. The thermal stresses accelerate tool fatigue and failures due to fracture, wear or chipping. Furthermore, if the temperature exceeds the crystal binding limits, the tool rapidly wears due to accelerated loss of bindings between the crystals in the tool material.

The history of cutting temperature research goes back as far as Taylor's experimental works in 1907. Taylor's experimental research lead to the understanding that increasing cutting speed decreased the tool life. Trigger and Chao [19] made the first attempt to evaluate the cutting temperature analytically. They calculated the average tool–chip interface temperature by considering the mechanism of heat generation during the metal cutting operations. They concluded that the tool–chip interface temperature is composed of two components: (a) that

* Corresponding author. Present address: Koc University, Istanbul, Turkey. Tel.: +1-90-212-338-1587; fax: +1-90-212-338-1548.
E-mail address: ilazoglu@ku.edu.tr (I. Lazoglu).

Nomenclature

α_n, β_n, ν Normal tool rake, normal friction and clearance angles
dx, dy Grid lengths along the x and y axes
$\delta\psi$ Angular increment of the tool grids
θ Cutter rotation angle
ρ Material density
τ, ϕ_n Shear stress and shear angle in the shear plane
ζ Thermal diffusivity
$[A]$ Square coefficient matrix of the chip heat equilibrium equations
χ Proportion of the shearing heat entering into the workpiece
Γ_i Proportion of the frictional heat entering into the tool at the ith nodal point
c Feed per revolution in turning, feed per tooth in milling
c_c Specific heat capacity of the chip
$\{C\}$ Heat generation array in the chip heat equilibrium equations
$[D]$ Square coefficient matrix of the tool heat equilibrium equations
dA Differential control zone
$\{E\}$ Heat generation array in the tool heat equilibrium equations
F_f Frictional force
F_s Shear force
h Instantaneous uncut chip thickness
k_t, k_c Thermal conductivity of the tool and chip
l_{cn} Tool–chip contact length
l Shear plane length
N_p Number of the angular divisions for the cutter meshes in the polar coordinates
N_x, N_y Number of the divisions for the chip meshes along the x, y axis (Fig. 2)
$\dot{Q}$ Heat conduction rates
$\dot{Q}_g$ Energy generation rate in the control volume (or in the control area in the 2-D)
R_t Thermal number
$\dot{Q}_s, \dot{Q}_f$ Rate of energy generated per unit depth of cut in the shear plane and along the tool–chip contact length, respectively
r_{max} Radius corresponding to the backside of the tool (at nodal point R)
s Nodal point number (at r_{max}) assigned to the tool on the rake face
$\{T_c\}, \{T_t\}$ Chip and tool temperature arrays
V_w, V_c, V_s Cutting, chip and shear velocities, respectively

due to the plastic deformation associated with the chip formation at the shear zone; and (b) that due to friction between the chip and tool face along the contact region. Loewen and Shaw [6] have stated that it is not possible to experimentally determine the influence of many of the variables on the cutting temperature, or to measure conveniently its components. They developed a simple analytical procedure to compute the interface temperature by making the assumptions that the fraction of heat flow into the chip is constant along the rake face in the tool–chip contact region, and the tool acts like a quarter-infinite body. Usui et al. [20] and Tlusty et al. [18] used the finite difference method to predict the steady-state temperature distribution in continuous machining by utilizing the predicted quantities, such as chip formation and cutting forces, through the energy method. The predicted temperatures were lower than the observed ones near the cutting edge and the chip leaving point. They

correlated the crater wear of carbide tools to the predicted temperature and stresses in the tool. Smith and Armarego [13] have predicted temperature in orthogonal cutting with a finite difference approach. Ren and Altintas [11] applied a slip line field solution proposed by Oxley [8] on high speed orthogonal turning of hardened mold steels with chamfered carbide and CBN tools. They evaluated the strain, strain rate and temperature dependent flow stress of the material, as well as the friction field at the rake face–chip contact zone from standard orthogonal cutting tests conducted with sharp tools. They showed a good correlation between the maximum temperature on the rake face and crater wear, which led to the identification of cutting speed limits for an acceptable tool life limits. Strenkowski and Moon [16] have developed an Eulerian finite element model to simulate the cutting temperature. This Eulerian formulation of the cutting model requires a constitutive law between the

viscosity, second invariant of the strain rate tensor and uniaxial yield stress. An iterative computational scheme is also required for the solution. Numerical solutions, especially Finite Element (FE) methods require accurate representation of material's constitutive properties during machining. However, since the strain rates and strains are several magnitudes higher than those evaluated from standard tensile and Hopkinson's bar tests, FE methods mainly suffer due to lack of accurate material models. Shatla et al. [12] used the material properties evaluated from orthogonal cutting and milling tests in the FE simulation of metal cutting. He reported improvements in predicting the temperature and cutting forces in both continuous turning and transient milling operations using a Finite Element method.

There has been less research reported in the prediction of tool temperature in milling, where the chip thickness vary continuously, and the process is intermittent (i.e., the tool periodically enters and exits the cut). As a result, the shear energy, shear angle, and the friction energy changes continuously with time. Hence, the process does not stay in steady-state equilibrium like in continuous machining operations. McFeron and Chao [7] have developed a model for the analytical calculations of average tool–chip interface temperature for the plain peripheral milling process. They have instrumented a face mill with a thermocouple to measure the average transient temperature on the rake face of a carbide tool. Stephenson and Ali [14] analyzed a special case of interrupted cutting with constant chip thickness. They have developed a model by considering a semi-infinite rectangular corner heated by a time varying heat flux with various spatial distributions to predict the average temperature on the rake face. They concluded that tool temperatures are generally lower in interrupted cutting than in continuous cutting under the same condition since temperature is dependent primarily on the duration of heating cycle and secondarily on the length of cooling time between cycles. As they noted, their analysis quantitatively underestimates the temperatures for short heating cycles. Stephenson et al. [15] have presented work on temperature prediction in contour turning. Redulescu and Kapoor [10] analyzed the tool–chip interface temperature by solving the heat conduction problem with prescribed heat flux. The mechanistic force model was utilized in this analysis. Their results also indicate that the tool–chip interface temperatures increases with cutting speed for both continuous and interrupted cutting. Jen and Lavine [3] used a similar approach to Redulescu for tool temperature calculation and improved calculation speed relatively by using power law approximation for the exponential terms. For further information on the literature review and on methods to calculate the machining temperature, the publication by Tay [17] is recommended.

One of the biggest challenge in this research area is the lack of the experimental data to verify the mathematical models proposed in predicting the tool temperature. It is rather difficult to embed sensors close to the cutting edge. Infra-red temperature sensors provide average readings from the entire cutting zone. When the cutting is time varying like in milling, it is more challenging to put even simple sensors close to the cutting edge of the rotating tool. Most published articles rely on the few published experimental data from Trigger and Chao [19], Boothroyd [2] and Stephenson et al. [14]. This paper also uses their measurements in verifying the proposed temperature prediction model in turning and milling.

In this work, the finite difference method is used for the predictions of steady-state tool and chip temperature fields and transient temperature variation in continuous machining and milling. Based on the first law of thermodynamics, heat balance equations are determined in partial differential equation forms for the chip in Cartesian coordinates and for the tool in the polar coordinates. Thereafter, the finite difference method is utilized for the solutions of the steady-state tool and chip temperature fields. In order to determine the transient temperature variation in the case of interrupted machining such as milling, the chip thickness is discretized along the time. Steady-state chip and tool temperature fields are determined for each of these discretized machining intervals. Based on thermal properties and boundary conditions, time constants are determined for each discrete machining interval. Based on knowledge of the steady-state temperature and time constants of the discretized first order heat transfer system, an algorithm is presented to determine the transient temperature variations. Simulation results for continuous and interrupted machining processes are presented and compared with the experimental data reported in the literature.

2. Modeling of heat generation and temperature distribution in machining

2.1. Heat generated in the primary and secondary deformation zones

It is assumed that the process has orthogonal cutting geometry and the chip is sheared from the blank at an infinitely thin shear plane (i.e. *primary deformation zone*). The chip slides on the rake face (i.e. *secondary deformation zone*) with a constant average friction coefficient. Heat generated per unit depth of cut in the primary and secondary zones are given as follows, respectively, [1]

$$\dot{Q}_s = F_s V_s = \frac{\tau h V_w \cos(\alpha_n)}{\sin(\phi_n)\cos(\phi_n - \alpha_n)} \dot{Q}_f = F_f V_c \qquad (1)$$

$$= \frac{\tau h V_w \sin(\beta_n)}{\cos(\phi_n + \beta_n - \alpha_n)\sin(\phi_n - \alpha_n)}$$

where F_s, F_f, V_w, V_s and V_c are the shear force in the shear plane, the frictional force between the tool rake face and the chip contact zone, the cutting velocity, the cutting velocity component along the shear plane and the cutting velocity component along the rake face, respectively. τ, ϕ_n, α_n and β_n are the shear stress in the shear plane, shear angle, normal rake angle and normal friction angle, respectively. h is the instantaneous uncut chip thickness (h=feed per revolution for turning, $h = c \cdot \sin(\theta)$ for end-milling, where c is the feed per tooth and θ represents the angular position of the cutting point).

The average temperature rise of the chip per unit depth of cut due to the shearing is determined by Oxley's energy partition function [8]

$$\Delta \bar{T} = \dot{Q}_s \cdot \frac{1-\chi}{\rho.c_c.h.V_w} \tag{2}$$

where ρ and c_c are the mass density and specific heat capacity of the chip, respectively. χ represents the proportion of the shearing flux entering into the workpiece, and is defined by:

$$\chi = 0.5 - 0.35 \log_{10}(R_t.\tan(\phi_n)) \text{ for } 0.004 \leq R_t.\tan(\phi_n) \leq 10$$
$$\chi = 0.3 - 0.15 \log_{10}(R_t.\tan(\phi_n)) \text{ for } R_t.\tan(\phi_n) \geq 10$$

(*thermal number*) $R_t = \dfrac{h.V_w}{\zeta}$, (*thermal diffusivity*) $\zeta = \dfrac{k_c}{\rho.c_c}$.

The average temperature rise on the shear plane is used as a boundary condition at Point D in Fig. 2, and the heat generated in the primary and secondary zones are used as heat sources in solving the temperature distribution within the tool and chip as presented in the following section.

2.2. Modeling and computational algorithm for steady-state chip–tool temperature fields

Based on the first law of thermodynamics, the energy balance in a two-dimensional (2-D) differential control zone can be written in Cartesian coordinates as:

$$\underset{\text{Heat Input}}{\dot{Q}_x + \dot{Q}_y} + \underset{\text{Heat Generated}}{\dot{Q}.dx.dy} \underset{\text{Heat Output}}{- \dot{Q}_{x+dx} - \dot{Q}_{y+dy}} \tag{3}$$

$$= \underset{\text{Heat Stored}}{\rho.c_p.\frac{\partial T}{\partial t}.dx.dy}$$

where $dx.dy$ is the area of the infinitesimal element zone. $\dot{Q}$, $(\dot{Q}_x, \dot{Q}_y)$ and $(\dot{Q}_{x+dx}, \dot{Q}_{y+dy})$ are the energy generation rate per unit area, the heat conduction input and output rates, respectively, which are perpendicular to the each control surface as shown in Fig. 1. ρ, c_p, t, T represent mass density, specific heat capacity of medium, time and the temperature in the element, respectively.
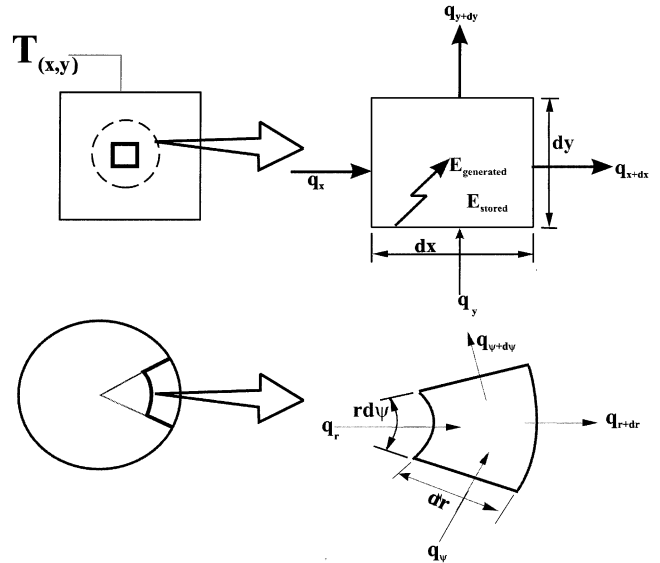

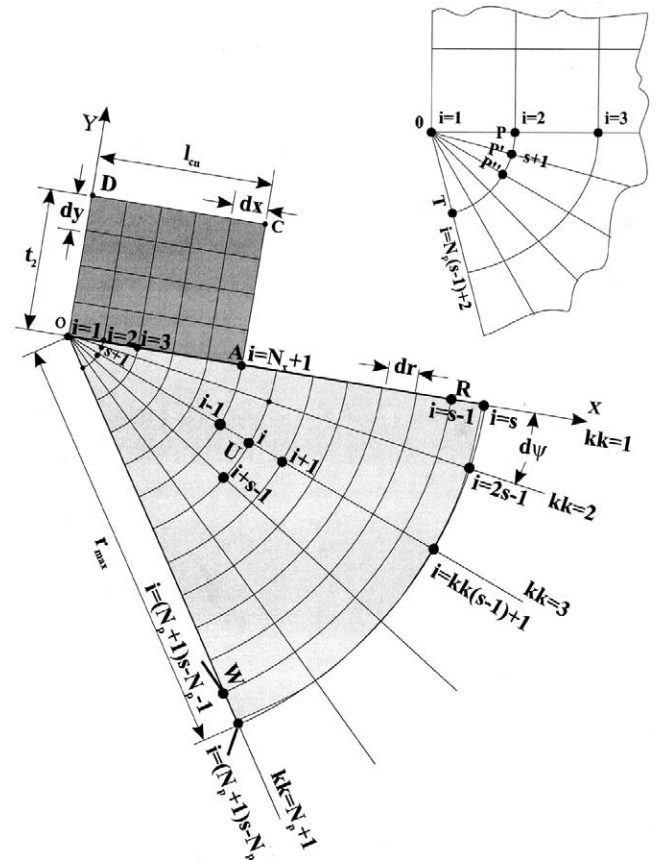Fig. 1. Heat diffusion in differential control zones defined in Cartesian and Polar Coordinates.

Fig. 2. Illustration of chip and tool meshing.

The heat conduction rates $(\dot{Q}_x, \dot{Q}_y)$ can be evaluated from Fourier's Heat Conduction Law,

$$\dot{Q}_x = -k.(dy).\frac{\partial T}{\partial x}, \dot{Q}_y = -k.(dx).\frac{\partial T}{\partial y} \tag{4}$$

where k is the thermal conductivity of the material. Using Taylor series expansion and ignoring the higher order terms, the heat flow rates in two orthogonal directions can be written as first order approximations:

$$\dot{Q}_{x+dx} = \dot{Q}_x + \frac{\partial \dot{Q}_x}{\partial x}dx, \dot{Q}_{y+dy} = \dot{Q}_y + \frac{\partial \dot{Q}_y}{\partial y}dy. \quad (5)$$

Assuming that the thermal conductivity does not vary in the medium, the heat balance can be rewritten as the following:

$$\frac{\partial^2 T}{\partial x^2} + \frac{\partial^2 T}{\partial y^2} + \frac{\dot{Q}}{k} = \frac{1}{\zeta}\frac{\partial T}{\partial t} \quad (6)$$

where ζ is the thermal diffusivity defined as $\frac{k}{\rho.c_p}$.

2.2.1. Chip temperature model

The chip can be considered as a medium which is in quasi-static thermal equilibrium during an infinitesimally small time. Considering orthogonal cutting (Fig. 2), with two-dimensional heat flow and one-dimensional mass transfer, the heat balance equation [as shown in Eq. (6)] for the discrete chip zone can be written in partial differential equation form in Cartesian coordinates as the following,

$$\left(\frac{\partial^2 T_c}{\partial x^2} + \frac{\partial^2 T_c}{\partial y^2}\right) + \frac{\dot{Q}_c}{k_c} = \left(\frac{\rho.c_c}{k_c}\right).\frac{\partial T_c}{\partial t} = \left(\frac{\rho.c_c}{k_c}\right).V_c\frac{\partial T_c}{\partial x} \quad (7)$$

where $\dot{Q}_c$, k_c, c_c are the energy generation rate per unit area in the differential chip zone, thermal conductivity and specific heat capacity of the chip, respectively. In the above equation, it should be noticed that $\frac{\partial T_c}{\partial t}$ can be replaced by $V_c\frac{\partial T_c}{\partial x}$. In order to solve the partial differential equation using the finite difference method, the following approximations can be made (Fig. 3),
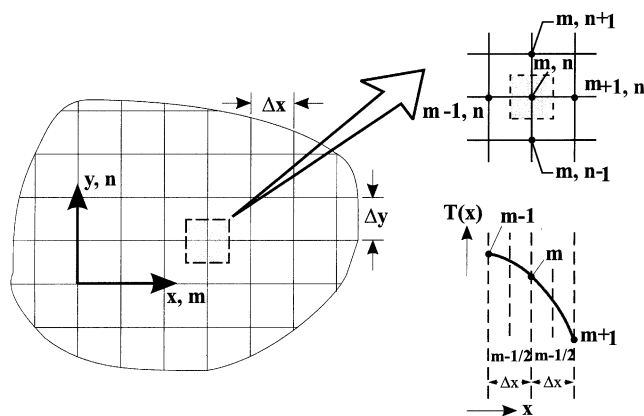

Fig. 3. Illustration of nodal network in 2-D control volume and Finite Difference Approximation.

$$\frac{\partial^2 T}{\partial x^2}\bigg|_{x,y} \simeq \frac{T_{(x+\delta x,y)} + T_{(x-\delta x,y)} - 2T_{(x,y)}}{\delta x^2}$$

$$\frac{\partial^2 T}{\partial y^2}\bigg|_{x,y} \simeq \frac{T_{(x,y+\delta y)} + T_{(x,y-\delta y)} - 2T_{(x,y)}}{\delta y^2}. \quad (8)$$

Therefore, by using the above approximations, the governing equation in the partial differential equation form (Eq. (7)) can be rewritten as in the following finite difference form:

$$\left(\frac{T_{c(x+\delta x,y)} + T_{c(x-\delta x,y)} - 2T_{c(x,y)}}{\delta x^2}\right.$$

$$\left. + \frac{T_{c(x,y+\delta y)} + T_{c(x,y-\delta y)} - 2T_{c(x,y)}}{\delta y^2}\right) + \frac{\dot{Q}_{c(x,y)}}{k_c} \quad (9)$$

$$= \frac{\rho.c_c}{k_c}.V_c\frac{\partial T_{c(x,y)}}{\partial x}.$$

The chip geometry must be meshed into small discrete elements for the finite difference solution of the chip temperature field and the equilibrium equation above needs to be written for each nodal point of the chip (Fig. 2). The aspect ratio of the mesh can be unity to simplify the solution, $\delta x = \delta y$.

In the equilibrium equation (Eq. (9)), the heat flow into the differential chip control zone ($\dot{Q}_c$) from the frictional heat source can be localized for each node along the chip–tool contact length as:

$$\dot{Q}_{c(i)} = \left. = \frac{(1-\Gamma_i).\dot{Q}_f.dx}{l_{cn}}\right\} \text{ if and only if } 1 \leq i \leq N_x \quad (10)$$
$$+ 1$$

where Γ_i represents the proportion of the frictional heat flowing into the tool at the ith nodal point and is unknown initially. $\dot{Q}_f$, l_{cn} and N_x are the frictional heat generation rate, chip–tool contact length and number of grids along the x axis, respectively. It should be noticed that a uniform heat generation was considered along the chip–tool contact length. The internal nodes (all nodes other than $1 \leq i \leq N_x+1$) will physically have no heat generation input. Therefore, $\dot{Q}_{c(i)}$ will be zero for all these nodes. Equilibrium equations for all of the nodes of the chip can be written as shown in Eq.(9), and all these equilibrium equations can be collected in a compact matrix form:

$$[\mathbf{A}].\{T_c\} = \{C\} \quad (11)$$

where $[\mathbf{A}]$ is the square coefficient matrix determined from Eq. (9), $\{T_c\}$ is the chip temperature array with size of $(N_y+1)(N_x+1)$ (where N_y is the number of meshes along the y axis as shown in Fig. 2), and $\{C\}$ is the heat generation array. The temperature of each nodal point in the chip nodal network corresponds to a value in the chip temperature array, $\{T_c\}$. $\{T_c\}$ can be determined as:

$$\{T_c\} = [A]^{-1}.\{C\}. \tag{12}$$

Writing the equilibrium equation for each nodal point $(1 \leq i \leq (N_y+1)(N_x+1))$ leads to the elements of coefficient matrix, $[A]$, and heat generation array, $\{C\}$.

2.2.2. Tool temperature model

Whereas Cartesian coordinates are used for the chip, applying polar coordinates to the tool is advantageous due to the mathematical accuracy and its convenience in the computational implementation of the model. Similar to the chip temperature model, the heat transfer equilibrium equations for the control zone around the tool nodal points can be written in the polar coordinates as,

$$\left(\frac{\partial^2 T_t}{\partial r^2} + \frac{1}{r}\frac{\partial T_t}{\partial r} + \frac{1}{r^2}\frac{\partial^2 T_t}{\partial \psi^2} \right) + \frac{\dot{Q}_t}{k_t} = 0 \tag{13}$$

where T_t represents the tool temperature field, r is the radial distance between the nodal point in concern and the tool tip shown as point O in Fig. 2, and ψ is the angular position of the nodal point. k_t and $\dot{Q}_t$ denote the tool thermal conductivity and heat generation rate per unit area in the control zone, respectively.

In order to write the above partial differential equation in the form of finite difference, the following approximations can be made:

$$\left. \frac{\partial^2 T}{\partial r^2} \right|_{r,\psi} \simeq \frac{T_{(r+\delta r,\psi)} + T_{(r-\delta r,\psi)} - 2T_{(r,\psi)}}{\delta r^2}$$

$$\left. \frac{1}{r}\frac{\partial T}{\partial r} \right|_{r,\psi} \simeq \frac{T_{(r+\delta r,\psi)} + T_{(r-\delta r,\psi)} - 2T_{(r,\psi)}}{2.r.\delta r} \tag{14}$$

$$\left. \frac{1}{r^2}\frac{\partial^2 T}{\partial \psi^2} \right|_{r,\psi} \simeq \frac{T_{(r,\psi+\delta\psi)} + T_{(r,\psi-\delta\psi)} - 2T_{(r,\psi)}}{r^2.\delta\psi^2}. \tag{15}$$

Therefore, the finite difference form of the tool heat balance equation (Eq. (13)) will be as the following;

$$\left(\frac{T_{t(r+\delta r,\psi)} + T_{t(r-\delta r,\psi)} - 2T_{t(r,\psi)}}{\delta r^2} \right.$$

$$+ \frac{T_{t(r+\delta r,\psi)} + T_{t(r-\delta r,\psi)}}{2r\delta r} \tag{16}$$

$$\left. + \frac{T_{t(r,\psi+\delta\psi)} + T_{t(r,\psi-\delta\psi)} - 2T_{t(r,\psi)}}{r^2\delta\psi^2} \right) + \frac{\dot{Q}_{t(r,\psi)}}{k_t} = 0.$$

The frictional heat flow rate into the tool is given by

$$\dot{Q}_{t(i)} = \left. \frac{\Gamma_i.\dot{Q}_f.dx}{l_{cn}} \right\} \text{ if and only if } 1 \leq i \leq N_x + 1. \tag{17}$$

Similar to the chip heat balance equations, the equilibrium equations for all nodal points of the tool can be written and collected in a compact form:

$$[D].\{T_t\} = \{E\} \tag{18}$$

where $[D]$ is the square coefficient matrix determined from Eq. (16), $\{T_t\}$ is the tool temperature array, $\{E\}$ is the heat generation array for the tool.

Therefore, the tool temperature distribution can be determined from

$$\{T_t\} = [D]^{-1}.\{E\} \tag{19}$$

The finite difference equilibrium equation of the tool (Eq. (16)) needs to be written for each nodal point of the tool. Thus, the elements of the tool coefficient matrix, $[D]$, and the heat generation array, $\{E\}$, can be determined for each tool node (for $1 \leq i \leq (N_p + 1)\left(\frac{r_{max}}{\delta r} + 1\right) - N_p$; where the number of discrete angles, $N_p = \frac{(\pi/2 - \gamma_n - \alpha)}{d\psi}$).

In the chip and tool heat balance equations, besides the tool and chip temperature distributions, the partitions of the heat (Γ_i) at the nodal points along the chip-workpiece contact length are also not known initially. Therefore, an iterative process is required for the computation. Initial values between 0 and 1 can be assigned for the heat partitions, Γ_i, at each nodal point. The tool and chip temperature fields can be determined based on the initial assignments of Γ_i. After solving the chip and tool heat balance equations (Eqs. (12) and (19)), if temperatures of the corresponding tool and chip nodal points, at which the tool and chip are in contact, are different than each other, then the heat partition value for the corresponding nodal points need to be modified. The following formulation can be employed for the partition modification,

$$d\Gamma_{(1:N_x+1)} = Gain.\frac{(T_{c(1:N_x+1)} - T_{t(1:N_x+1)})}{\dfrac{(T_{c(1:N_x+1)} + T_{t(1:N_x+1)})}{2}}. \tag{20}$$

The above equation compares the difference between the chip and tool temperatures at every nodal point, at which chip and tool is in contact, with their average temperature. Initial value of *Gain* may be set to unity; if numerical divergence occurs during the solution, its value should be decreased to guarantee convergence at the cost of computation time.

If the *maximum* of $d\Gamma_{(1:Nx+1)}$ is greater than a certain predefined percentage, then the new heat partition values for the corresponding nodes can be assigned as

$$\Gamma_i = \Gamma_i + d\Gamma_i \text{ for } 1 < i < N_x + 1. \tag{21}$$

With these new heat partitions, the finite difference equations for the chip and tool are solved again and $d\Gamma_{(1:Nx+1)}$ values are redetermined. The new partition should allow the temperature fields of the tool and chip at the contact region to converge. This iterative solution will continue until *maximum* of $d\Gamma_{(1:Nx+1)}$ reaches to a predefined satisfactory low level. Thus, at the end of the

iterative solution, the temperature fields of the tool and chip can be determined from $\{T_t\}$, $\{T_c\}$.

3. Modeling of transient temperature variation in milling

In the previous sections, the methodology and computational algorithm to determine the *steady-state* tool and chip temperatures was described. However, it is also important to know transient temperature variations, especially for the high-speed interrupted machining processes, such as milling in which flute and workpiece contact is not continuous and the uncut chip thickness varies with the spindle rotation (i.e. with time). The temperature on a flute rises during the cutting process due to generated shear and frictional heat and decreases during the non-cutting period due to the forced convection of the cutting fluid or the air.

It is well known that the heat transfer system is physically a first order system. Therefore, besides knowing the steady-state temperatures, knowledge of the time constant of the system will be sufficient to predict the transient response of the system. By utilizing the finite difference algorithm shown in the previous section, the steady-state temperatures can be determined for a given set of system inputs. Therefore, the problem to determine the transient response of the system, is reduced to determine the time constant of a given system. Ozisik [9] has given the transient temperature solution for a rectangular parallelpiped with zero temperature boundary conditions and a known initial temperature field. It can be seen from this solution that the transient response of the heat transfer problem is governed by $e^{-\zeta(\beta_m^2 + \gamma_n^2 + \eta_p^2)}$ where β_m, γ_n and η_p are the roots of $\sin(\beta_m i)=0$, $\sin(\gamma_n j)=0$, $\sin(\eta_p k)=0$ (i.e., $\beta_m = \dfrac{m\pi}{i}$ for $m=1,2,3,...$; $\gamma_n = \dfrac{m\pi}{j}$ for $n=1,2,3,...$; $\eta_p = \dfrac{m\pi}{k}$ for $p = 1,2,3,...$ where i,j,k are the dimensions of the rectangular parallelpiped). Therefore, the first eigenvalue ϖ^2 is approximated ([10]) as

$$\varpi^2 \simeq \zeta\left(\frac{\pi^2}{i^2} + \frac{\pi^2}{j^2} + \frac{\pi^2}{k^2}\right). \tag{22}$$

Considering orthogonal cutting, and by utilizing the first eigenvalue for the chip formation zone, it can be seen that the transient response of the heat transfer problem is governed by $e^{-\frac{t}{\tau}}$ where $\tau\left(= \dfrac{1}{\varpi^2}\right)$ is the time constant, and τ can be approximately determined from

$$\tau \simeq \frac{1}{\zeta\cdot\left(\dfrac{\pi^2}{l_{cn}^2} + \dfrac{\pi^2}{l^2}\right)} \tag{23}$$

where ζ is the thermal diffusivity of the chip/workpiece

defined as $\dfrac{k_c}{\rho.c_c}$. l_{cn} is the tool-chip contact length, and l is the shear plane length given by,

$$l_{cn} \approx \frac{2.h.\sin(\phi_n + \beta_n - \alpha_n)}{\cos(\beta_n).\sin(\phi_n)}, l = \frac{h.\cos(\phi_n - \alpha_n)}{\sin(\phi_n)}.$$

Therefore, after determining the steady-state temperature and time constant, the variation of the tool–chip transient contact temperature can be easily determined for constant chip thickness machining processes such as turning.

Alternately, for the cases in which the chip thickness varies with time, such as in milling, the chip thickness can be discretized into constant sections as shown in Fig. 4 and each section is now considered like a turning process for a discrete machining time of $\Delta t \left(= \dfrac{\Delta\theta}{2\pi rpm}\dfrac{60}{}\right)$. Then, the steady-state temperatures $[(T_{ss})_i]$ and corre-
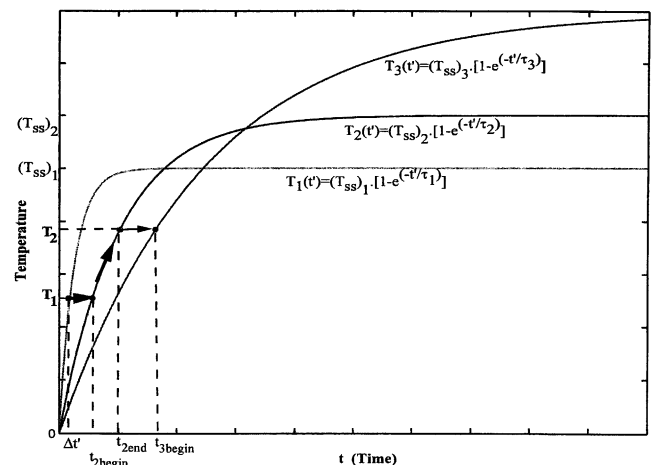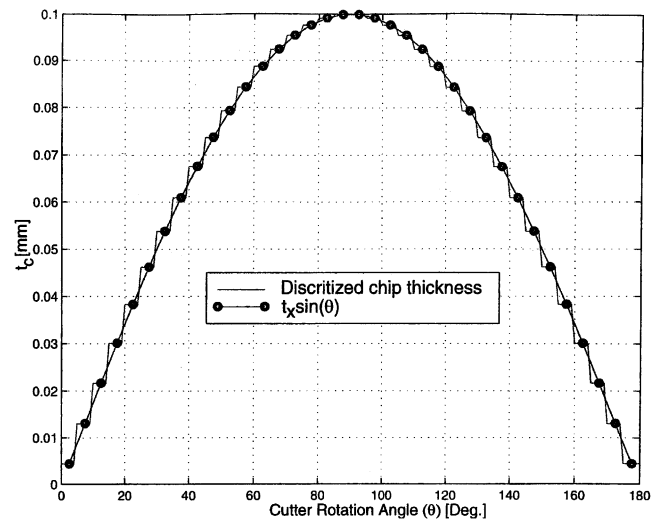

Fig. 4. Illustration of the chip thickness discritization for end milling and temperature prediction procedure for the machining with variable thickness.

sponding time constants (τ_i) for every ith discrete chip thickness (in other words, for each discrete cutter rotation angle) can be determined as explained in the previous lines. Using a simple analysis of the first order systems, transient response can be also determined:

$$T_1(t) = (T_{ss})_1 \cdot \left(1 - e^{-\frac{t}{\tau_1}}\right) \tag{24}$$

where $(T_{ss})_1$ and τ_1 are the steady-state temperature and the time constant corresponding to the first discrete chip thickness cut after $\Delta\theta$ angular rotation of the milling tool. t is the machining time, and for the first discrete chip thickness, it varies between zero and Δt, which is the machining time interval corresponds to a discrete chip thickness. Selection of smaller time increments (Δt) will increase the computation time but allows greater accuracy in the predictions. The temperature reaches to the following value at the end of Δt,

$$T_1 = T_1(\Delta t) = (T_{ss})_1 \cdot \left(1 - e^{-\frac{\Delta t}{\tau_1}}\right). \tag{25}$$

After determining the temperature for the first discrete chip thickness, the system can be considered as 'frozen' in time. Then the system is started, with the initial temperature of T_1, to turn at the second discrete chip thickness. After machining at the second discrete chip thickness, Δt time later, the temperature will reach to

$$T_2 = (T_{ss})_2 \cdot \left(1 - e^{-\frac{t_{2end}}{\tau_2}}\right) \tag{26}$$

where $t_{2end} = t_{2begin} + \Delta t$

$$t_{2begin} = -\tau_2 \ln\left[1 - \frac{T_1}{(T_{ss})_2}\right]$$

and $(T_{ss})_2$ is the steady-state temperature evaluated from the continuous machining model presented in the previous section. More generally, the temperature for ith discrete chip thickness can be found as:

$$T_i = T_{ss(i)} \cdot \left(1 - e^{-\frac{time\ end(i)}{\tau_i}}\right) \tag{27}$$

where

$$time\ end(i) = time\ begin(i) + \Delta t$$

$$time\ begin(i) = -\tau_i \cdot \ln\left[1 - \frac{T_{(i-1)}}{T_{ss(i)}}\right]$$

An illustration to determine the transient temperature for discretized chip thickness is shown in Fig. 4. The above technique allows to determine the temperature at every Δt time interval which corresponds to a discrete cutter rotation angle.

4. Simulation results and discussions

In this section, the simulation results based on the proposed model are presented, and compared against the widely accepted but rarely found experimental temperature data published in the literature.

4.1. Continuous machining tests

Boothroyd [2] used infra-red photographic techniques to measure the temperature of a pre-heated tubular workpiece which was end-machined on a lathe. Orthogonal cutting conditions with the feed per revolution of 0.604 mm/rev were performed on a mild steel tube with an outside diameter of 63.5 and 6.35 mm wall thickness. Boothroyd indicated that measurements of the width of the chip after machining did not show an increase in the width of chip exceeding 4% of the original width and the average increase was 2.2%. Due to this result, plane strain conditions could be assumed. He presented the measured isotherm patterns on the chip and on the workpiece at a cutting speed of 22.86 m/min, a tool rake angle of 30°, and clearance angle of 7°, the pre-heating temperature of the workpiece was 611 °C. The shear angle was calculated as 40.5 degrees from ratio of the given chip thicknesses using the geometric relationship [1]. The temperature rise due to the shear was calculated as 169.4 °C from Eq. (2). Simulation was performed for the same cutting conditions using workpiece conductivity, density and thermal capacity of 42.6 W/(m·K), 7850 kg/m³, 473 J/(kg·°C), respectively, for the mild steel. Tool conductivity, density and thermal capacity were 28.4 W/(m·K), 11100 kg/m³, 276 J/(kg·°C), respectively. For the finite difference solution, N_y, N_p and $d\Gamma_{max}$ were set to 10, 8 and 3%, respectively. The simulated chip and tool temperature isotherm patterns are given in Fig. 5. Boothroyd reported that the maximum temperature
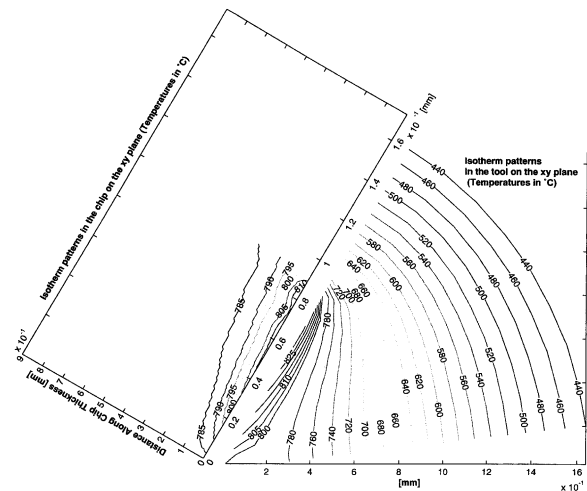
Fig. 5. Predicted isotherms patterns of the chip during the machining of mild steel under the conditions given by Boothroyd [2] (temperatures in °C).

measured on the rake face was around 760 °C, and the simulation results show the maximum temperature as 810 °C. The simulations show slightly higher temperature close to the shear zone (785 °C) as opposed to 660 °C reported by Boothroyd. The small discrepancies may be attributed to the preheating of the tube (611 °C) by Boothroyd, which could have changed the properties of the mild steel workpiece. In general the simulated magnitudes and traces of isotherms are quite similar, although the tool edge geometry and actual material properties may be slightly different than those used by Boothroyd.

Stephenson and Ali [14] measured temperature during the continuous and interrupted turning of Al2024-T351 tubes by using a tool–chip thermocouple method. The tool was a standard C2 WC tool. The first set of the experimental tests was performed by continuous cutting and the average measured temperature was 280 °C. In this test, cutting speed, feed per revolution, cutting force, feed force and cut chip thickness were 1.36 m/s, 0.165 mm, 573 N, 329 N and 0.333 mm. The width of cut was 2.54 mm. The rake and inclination angles were zero. Based on the previous experiments, they assumed that the chip–tool contact length was given to be 1.5 times the cut chip thickness. Simulation was performed for this cutting conditions using workpiece conductivity, density and thermal capacity of 177 W/(m·K), 2700 kg/m^3, 613 J/(kg·°C), respectively, for Al2024-T351. Tool conductivity, density and thermal capacity were 28.4 W/m-K, 11100 kg/m^3, 276 J/(kg·°C), respectively. The shear angle was determined from the chip ratio as 26.4 degrees. The friction angle was determined as 29.8 degrees from the measured cutting and feed force values. The temperature rise due to the shear was calculated as 215 °C from Eq. (2). For the finite difference solution, N_y, N_p and $d\Gamma_{max}$ were set to 10, 8 and 3%, respectively. The predicted steady-state average temperature was found to be 283 °C, which is very close to 280 °C measured by Stephenson and Ali. The temperature fields of the chip and tool and the variation of partition of the heat flux which flows into the tool along the chip–tool contact region on the rake face for this continuous cutting conditions are also illustrated in Figs. 6 and 7, respectively. The maximum tool temperature is predicted to be about 370 °C and it occurs at about 0.4 mm away from the cutting edge. The total chip contact length is about 0.525 mm and the uncut chip is about 0.165 mm. It is interesting to observe in Fig. 7 that close to the end of the contact region (~0.5 mm), most of the heat flux flows into the tool. Γ_i may sometimes be larger than 100%. This phenomena was observed also by McFeron and Chao [7]. This indicates that not only the frictional energy transferred to the tool but also some of the chip heat is transmitted to the tool in order to balance relatively cold tool backside temperature.

Strenkowski and Moon measured average temperature at the rake face–chip contact zone by instrumenting the tool with thermocouples [16]. They turned Al6061-T6 tubes with a high speed steel tool at different cutting speeds, feedrates and rake angles. Simulation was performed for the same cutting conditions and work material using workpiece conductivity, density and thermal capacity of 204 W/(m·K), 2700 kg/m^3, 896 J/(kg·°C), respectively. Tool conductivity, density and thermal capacity were 42.6 W/(m·K), 7858 kg/m^3, 612 J/(kg·°C), respectively. For the case with the feed per revolution of 0.0635 mm/rev and the rake angle of 30 degrees, the shear angle, the friction angle and the temperature rise due to the shear were calculated as 28.3 degrees, 37.1 degrees and 66.5 °C, respectively. For the case with the feed per revolution of 0.127 mm/rev and the rake angle of 0 degree, the shear angle, the friction angle and the temperature rise due to the shear were calculated as 21.2 degrees, 25.7 degrees and 99 °C. For the finite difference solution, N_y, N_p and $d\Gamma_{max}$ were set to 8, 8 and 5%, respectively. As seen in Fig. 8, the simulation results and experimental measurements agree well.

4.2. Interrupted machining tests

The transient changes in the temperature can be verified using interrupted turning and milling tests. In interrupted turning, a slot is opened in the turned shaft, and the chip thickness is constant. However, the tool enters and exits the work material periodically, experiencing heating and cooling that leads to the transient changes in the temperature. In milling however, not only does the tool periodically engage and disengage, the tool also experiences time varying chip load. Hence, the energy created in the primary and secondary zones varies with time.

Stephenson and Ali also measured the temperature during the two sets of interrupted turning of A2024-T351 pronged slotted tubes with cut length of 51 mm and non-cut (slot) length of 9 mm. In this test, the cutting speed, feed per revolution, cutting force, feed force and cut ship thickness were 1.36 m/s, 0.109 mm, 393 N, 238 N and 0.262 mm. The measured steady-state temperature for these cutting conditions was found to be 255 °C. The proposed transient temperature model predicted the average temperature as 250 °C with 0.24 ms rise time (Fig. 9), which are quite comparable with the Stephenson's measurement. Radulesco and Kapoor [10] have also performed simulations based on the same cutting conditions and have also noted that the time required to reach steady state was 0.20 ms. In the interrupted cutting cases, the proposed model predicted and experimental results agree well.

McFeron and Chao [7] measured the average tool–chip interface temperature using a thermocouple technique in peripheral milling. The workpiece material was AISI 4140 steel. The insert grade was K3H carbide with
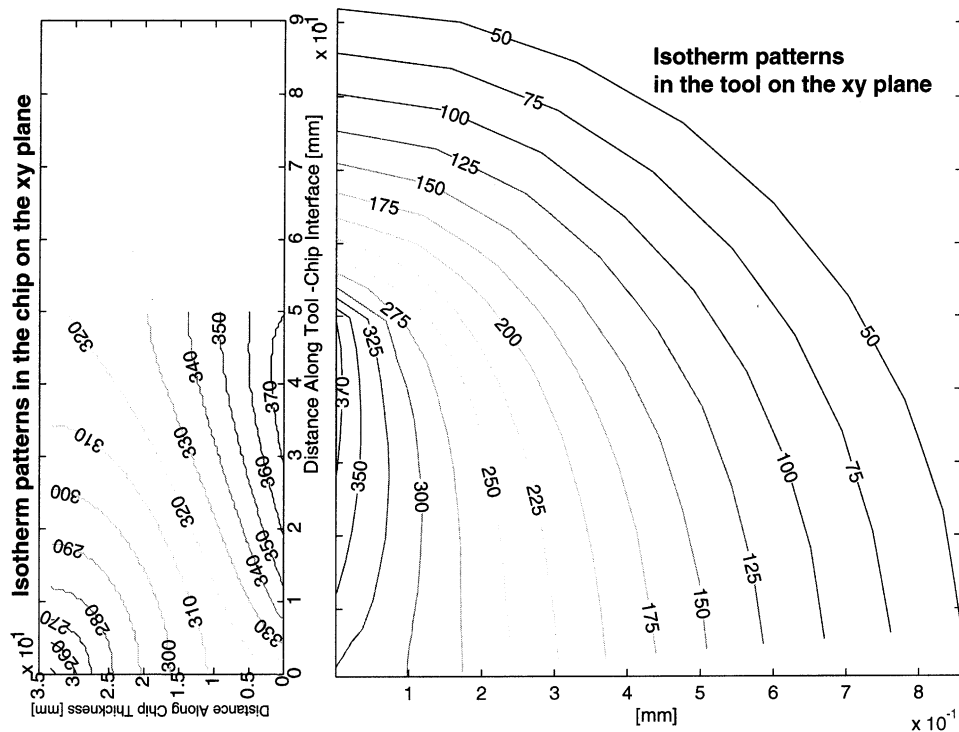
Fig. 6.   Isotherm patterns of the steady-state chip and tool temperature in (°C) fields during the machining of A12024.
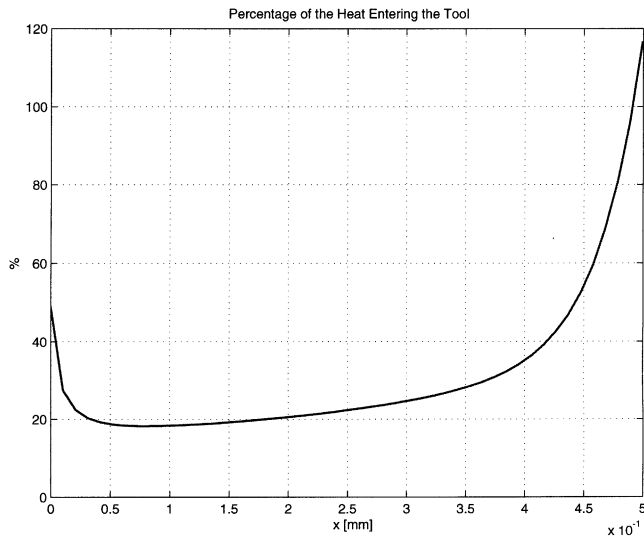

Fig. 7.   Variation of the portion of heat flux that flows into the tool along the chip–tool contact region on the rake face.
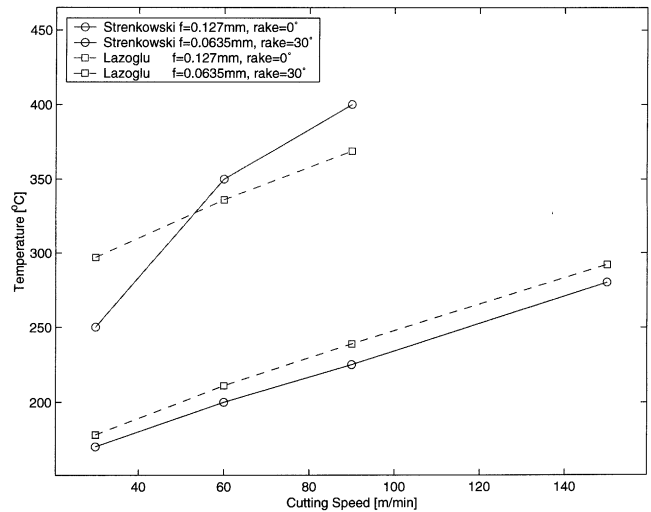

Fig. 8.   Variation of average interface temperature with cutting speed and feed per revolution (Strenkowski's measured temperature vs Lazoglu & Altintas's model predictions) for A16061.

0 degree rake angle and 6 degrees clearance angle. Cutter diameter, depth of cut, angle of contact and feed per tooth were 261.62 mm, 1.27 mm, 8 degrees and 0.113 mm, respectively. Simulation was performed for the AISI 4140 workpiece (conductivity, density and thermal capacity of 42.6 W/(m·K), 7850 kg/m^3, 473 J/(kg·°C), respectively). Tool conductivity, density and thermal capacity were 28.4 W/(m·K), 11100 kg/m^3, 276 J/(kg·°C), respectively. The given chip ratios for each cutter rotation angle, {0.22, 0.27, 0.30, 0.32, 0.34, 0.36,

0.37}, and given average shear flow stress of 1150 MPa were utilized in the simulation program. For the finite difference solution, N_y, N_p and $d\Gamma_{max}$ were set to 8, 8 and 3%, respectively. The measurement results in [7] for 80.46 m/min cutting speed and corresponding simulation predictions are shown in Fig. 10. Although the simulation result underpredicts the average interface temperature in the beginning of the cutter rotation, it agrees well with the experimental results as cutter rotation increases. Underprediction of temperature in the early stage of the
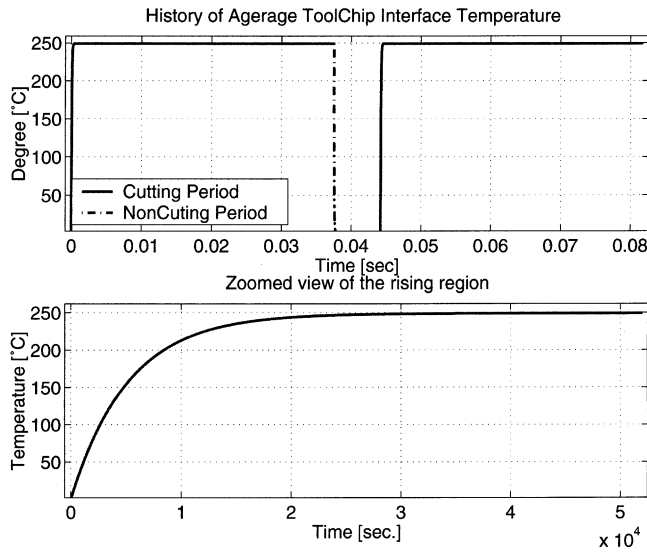
Fig. 9. Predicted average tool–chip interface temperature for the interrupted turning of A12024 (cutting interval time=0.0375s, non-cutting interval time=0.0067s).
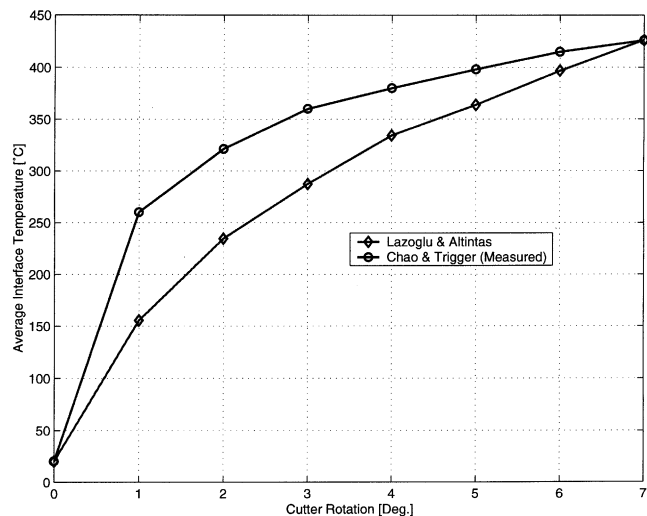

Fig. 10. Measured and predicted average chip–tool interface temperature during milling AISI 4140 [7].

cutter rotation may be due to improper prediction of the shear plane temperature which is highly dependent on the uncut chip thickness (Eq. (2)).

5. Conclusions

In this paper, starting from the first law of thermodynamics, a numerical model based on the finite difference method was presented for the predictions of steady-state tool and chip temperature fields and for transient temperature variation in continuous and interrupted orthogonal machining processes with varying chip load, such as in milling.

Heat balance equations were determined in partial dif-

ferential equation forms for the chip and for the tool. the finite difference method was utilized for the solutions of the steady-state tool and chip temperature fields. In order to determine the transient temperature variation in the case of interrupted machining, the chip thickness was discretized along the time. Steady-state chip and tool temperature fields were determined for each of these discretized machining intervals. Based on thermal properties and boundary conditions, time constants were determined for each discrete machining interval. By knowing the steady-state temperature and time constants of the discretized first order heat transfer system, an algorithm was presented to determine the transient temperature variations in interrupted turning and milling operations.

Simulations were performed for different materials under various cutting conditions. The results both for continuous and interrupted machining processes agreed well with experimentally measured temperatures.

The simulation of steady state and temperature distribution at the tool rake face has two important uses in high speed machining of metals. The tool should not be used close to and beyond the diffusion and bonding limits of materials used in the specific tool grade. For example, the diffusion limit for the Cobalt binding in Tungsten Carbide tools is about 1100–1200 °C. The same limit is about 1600–1800 °C for Cubic Bron Nitride (CBN) tools depending on the specific grades. If the tool experiences temperature beyond this limit, it rapidly wears [11]. Hence, the cutting conditions must be selected in such a way that the predicted temperature does not exceed this limit.

End mills and inserted milling cutters with small diameters are used in high speed milling of dies and molds, where the high temperature is a severe constraint in tool life. Similarly, heat resistant alloys such as titanium and nickel alloys limit the cutting speed due to accelerated wear and chipping of the cutting edges due to thermal loading of the tool. In both cases, the chip load and the cutter immersion periods (i.e. radial width of cut) must be selected in such a way that the cutter leaves the cut before the maximum tool temperature reaches a tool binding temperature limit. For example, titanium alloys are always cut with a very small radial immersion at high speeds in order to leave the cut before the temperature rises to the dangerous level.

The proposed algorithm can be utilized in selecting cutting speed, feed rate and tool rake and clearance angles in order to avoid excessive thermal loading of the tool, hence reducing the edge chipping and accelerated wear of the cutting tools.

Acknowledgements

Motors Canada and Boeing Corporations. Tools are provided by Mitsubishi Materials Corporation.

References

[1] Y. Altintas, Manufacturing Automation: Metal Cutting Mechanics, Machine Tool Vibrations, and CNC Design, Cambridge University Press, Cambridge, UK, 2000.

[2] G. Boothroyd, Temperatures in orthogonal metal cutting, Proceedings of the Institution of Mechanical Engineers 177 (29) (1963) 789–803.

[3] T.C. Jen, A.S. Lavine, Prediction of Tool Temperatures in Cutting, in: Proceedings of the Seventh International Symposium on Transport Phenomena in Manufacturing 1994, pp. 211–216.

[4] F. Klocke, W. Konig, Gerschwiler, Advanced Machining of Titanium and Nickel-Based Alloys, Advanced Manufacturing Systems and Technology, Springer Verlag, New York, USA, 1996.

[5] P. Lezanski, M.C. Shaw, Tool face temperatures in high speed milling, Transactions of ASME, Journal of Engineering for Industry 112 (1990) 132–135.

[6] E.G. Loewen, M.C. Shaw, On the Analysis of Cutting-Tool Temperatures, Transactions of ASME, Journal of Engineering for Industry 76 (1954) 217–231.

[7] D.E. McFeron, B.T. Chao, Transient interface temperatures in plain peripheral milling, Transactions of ASME, Journal of Engineering for Industry 80 (1958) 321–329.

[8] P.L.B. Oxley, Mechanics of Machining: An Analytical Approach to Assessing Machinability, John Wiley & Sons, New York, USA, 1989.

[9] M.N. Ozisik, Heat Conduction, second ed, John Wiley and Sons, New York, USA, 1993.

[10] R. Radulescu, S.G. Kapoor, An analytical model for prediction of tool temperature Fields during continuous and interrupted cutting, Transactions of ASME, Journal of Engineering for Industry 116 (1994) 135–140.

[11] H. Ren, Y. Altintas, Mechanics of machining with chamfered tools, Trans. ASME, Journal of Manufacturing and Engineering and Science 122 (2000) 650–659.

[12] M. Shatla, Y.C. Yen, O. Castellanos, L. Menegardo, T. Altan, T, Prediction of Cutting Forces, Temperatures and Stresses from Flow Stress Data and Cutting Conditions—Research in Progress, in: Proceedings of the Second CIRP International Workshop on Modeling of Machining Operations, Ecole Centrale De Nantes, Nantes, France, January 25-26, 1999.

[13] A.J.R. Smith, J.A. Armarego, Temperature prediction in orthogonal cutting with a finite difference approach, Annals of CIRP, 1981.

[14] D.A. Stephenson, A. Ali, Tool temperatures in interrupted metal cutting, Transactions of ASME, Journal of Engineering for Industry 114 (1992) 127–136.

[15] D.A. Stephenson, T.C. Jen, A.S. Lavine, Cutting tool temperatures in contour turning: transient analysis and experimental verification, ASME, Journal of Manufacturing Science and Engineering 119 (1997) 494–501.

[16] J.S. Strenkowski, K.-J. Moon, Finite element prediction of chip geometry and tool/workpiece temperature distributions in orthogonal metal cutting, Transactions of ASME, Journal of Engineering for Industry 112 (1990) 313–318.

[17] A.A.O. Tay, A review of methods of calculating machining temperature, Journal of Materials Processing Technology 36 (1993) 225–257.

[18] J. Tlusty, E. Orady, Effect of Thermal Cycling on Tool Wear in Milling, in: 9th NAMRC Conf., Penn. State University, May 1981.

[19] K.J. Trigger, B.T. Chao, An Analytical Evaluation of Metal Cutting Temperatures, Transactions of ASME 73 (1951) 57–68.

[20] E. Usui, T. Shirakashi, T. Kitagawa, Analytical prediction of three dimensional cutting process, Part 3: Cutting temperature and crater wear of carbide tool, Transactions of ASME, Journal of Engineering for Industry 100 (1978) 236–243.